Rotator Phases and Surface Crystallization in α-Eicosene

Hu Gang,[†] Oleg Gang,[‡] Henry H. Shao,[†] X. Z. Wu,[§,⊥,#] Jay Patel,[§] C. S. Hsu,[†] M. Deutsch,[‡] B. M. Ocko,[||] and E. B. Sirota*[,†]

Exxon Research and Engineering Co., Route 22 East, Annandale, New Jersey 08801; Physics Department, Bar Ilan University, Ramat Gan 52900, Israel; Physics Department, Northern Illinois University, DeKalb, Illinois 60115; Materials Sciences Division, Argonne National Laboratory, Argonne, Illinois 60439; and Physics Department, Brookhaven National Laboratory, Upton, New York 11973

Received: December 30, 1997

The rotator phases and surface crystallization of α-eicosene were studied using surface and bulk X-ray scattering techniques as well as surface tensiometry. The α-olefin differs from the *n*-alkane in a weak breaking of the molecular inversion symmetry. Behavior qualitatively the same as, but quantitatively different from, the corresponding *n*-alkane was observed. The temperature range of stability of the bulk rotator and surface crystal phases was enhanced. The broken inversion symmetry of the molecule did not manifest itself in the nature of these phases.

Introduction

Since the alkyl chains are a major building block of many other organic compounds, the properties of *n*-alkanes have been extensively studied. Two phenomena that have been recently probed in great depth in the alkanes have been the rotator phases,[1−15] which occur below the melting temperature T_m, and surface crystallization,[16−22] which occurs immediately above the melting temperature. The rotator phases are crystalline phases lacking long-range order in the rotation of the molecular plane about the molecular long axis. They are characterized by a strong temperature dependence of their structural and thermal properties. The surface crystallization phenomenon is the spontaneous formation of a crystalline monolayer, usually of a rotator phase, at the surface. This monolayer is in equilibrium with the underlying bulk liquid over a temperature range of a few degrees above the melting temperature.

It is important to understand how the properties of the alkanes carry over to derivative molecules.[23] Are the above "novel" phenomena only properties of *n*-alkanes, or are they more general? Do various derivatizations of the alkanes affect certain properties more than others? It is already known that these phenomena exist in alkane mixtures as well as pure alkanes, with the rotator phases playing an even larger role in the mixtures.[3,24−26] Recent studies of l-alcohols have shown how the rotator phases[27] and surface crystallization[28−30] carry over to those systems, where asymmetry of the molecule drives the system from a structure consisting of monolayers to structures consisting of bilayers, while preserving the main features of these phases.

In the current work we used X-ray scattering and surface tension to characterize an α-olefin, α-eicosene $CH_3-(CH_2)_{17}-CH=CH_2$ (denoted henceforth αC20), which differs from *n*-eicosane, the 20-carbon *n*-alkane (denoted nC20), by the presence of a double bond at one of the terminal carbons. The melting temperature of this material is ∼10 °C below that of the alkane. We find that αC20 shows rotator phases and surface crystal phases both with temperature ranges larger than those in nC20. The properties of these phases are quantitatively, but not qualitatively, different from those of the alkanes. We find no evidence for bilayer formation in the temperature range studied, either in the bulk or at the surface. This is contrary to what might be expected from a molecule where the inversion symmetry is broken, like we find in alcohols.[27−30] This may be attributed to the much weaker asymmetry of the α-olefin, compared to a 1-alcohol, as well as the competition with entropic disorder which would favor maintaining the inversion symmetry of the molecules in any given structure.

TABLE 1: Composition (wt %) of the Aldrich Eicosene (α-C20 olefin) Determined by GC-MS[a]

89.4%	1-C20 olefin	2.2%	1-C22 olefin
1.5%	1-C18 olefin	0.5%	*x*-C22 olefin
5.8%	*x*-C20 olefin		

[a] *x* small but >1, i.e., not terminal still close to the end.

Experimental Section

The eicosene sample was obtained from Aldrich, labeled 90% pure, and used as obtained. For *n*-alkanes, the impurities are usually neighboring homologues. To be sure, GC-MS analysis was performed to identify the impurities.[31] The results are given in Table 1. These were the neighboring even-chain-length homologues of the α-olefin as well as those chain lengths with the olefin near the α position. On the basis of previous studies of binary mixtures of *n*-alkanes,[25,29,32] we do not expect this quantity of these neighboring impurities to dramatically effect the properties.

DSC was performed on a Seiko RDC220 Robotic DSC.[27] Surface tension measurements were performed using the Wilhelmy plate method.[17,18] X-ray scattering on the bulk powder samples were performed using a Rigaku 18 kW rotating anode generator with a Huber goniometer.[8] X-ray reflectivity (XR) and grazing incidence diffraction (GID) from the liquid surface

* Corresponding author. E-mail: ebsirot@erenj.com.
[†] Exxon Research and Engineering Co.
[‡] Bar Ilan University.
[§] Northern Illinois University.
[⊥] Argonne National Laboratory.
[||] Brookhaven National Laboratory.
[#] Present address: IBM Almaden Research Center, 650 Harry Road, San Jose, CA 95120-6099.

S1089-5647(98)00603-8 CCC: $15.00
Published on Web 03/20/1998

was performed on the Harvard/BNL liquid surface spectrometer at beamline X22B of the National Synchrotron Light Source and Brookhaven National Laboratory.[17] The details of the various experimental techniques and methods of data analysis are well-established, and their details are discussed elsewhere.[8,17]

Bulk Properties

The eicosene freezes into and melts from the hexagonal R_{II} rotator phase at about 26.5 °C. At 22 °C there is a weak first-order transition to the orthorhombic R_I rotator phase which is characterized by a distortion of the average unit cell from hexagonal. This distortion can be quantified in terms of the order parameter $\xi = (a^2 - b^2)/(a^2 + b^2)$ where a and b are the major and minor axes of an ellipse drawn through the six nearest neighbors of a molecule.[8,23,33] Thus $\xi = 0$ in the hexagonal R_{II} phase. At 2 °C is a transition to the orthorhombic crystal phase characterized by long-range herringbone order of the backbone planes. This sequence of phase transitions appears to be a generic primary feature of alkane-chain-based molecules, with additional order parameters such as tilt magnitude and direction being of secondary importance.[23]

The DSC measurement of the melting transition was performed both heating and cooling at 1 °C/min. On cooling, freezing indicated by deviation from the baseline occurred at 26.1 °C. The DSC melting peak on heating occurred at 28.5 °C. The melting point of 26.5 °C, measured with X-ray scattering with 30 min equilibration, is consistent with these numbers. The heats of melting and of transition between the rotator and crystal phases were 39.8 and 5.2 kJ/mol, respectively, each with a possible 5% systematic error. This heat of melting is lower than the value interpolated for nC20 and close to the interpolated value for this transition in nC18.[34] (Interpolation is necessary to obtain comparative values for the even *n*-alkanes since they exhibit direct liquid-to-crystal transitions without the intervening rotator phase.) The heat of the rotator−crystal transition is substantially lower than that observed in pure *n*-alkanes (∼13.7 kJ/mol).[34] This is not surprising since, as occurs in mixtures of *n*-alkanes,[25] an extended rotator phase range with a higher heat capacity than both the liquid and crystal phases has been shown to tend to decrease the latent heat of the rotator−crystal transition.

The layer spacing is determined by the 00l reflections where $q_{00l} = 2\pi l/d$. We determined $d = 27.26$ Å with a thermal expansion of $(1/d)(\mathrm{d}d/\mathrm{d}T) < 2 \times 10^{-4}$ °C^{-1} and no observable discontinuities at either solid−solid transition. For the nC20, $d = 27.7$ Å in the untilted rotator phases. Since the crystal phase of *n*-eicosane is a tilted triclinic crystal, we can interpolate the values for C19 and C21 *n*-alkanes in their orthorhombic crystal phase[34] and obtain $d = 27.4$ Å. The value for αC20 is thus consistent with the molecules being perpendicular to the layers in all three solid phases. We carefully looked for evidence of a peak at half-integer multiples of $2\pi/d$, which would be present if a bilayer structure occurred. No evidence of such bilayer ordering was observable to temperatures down to −10 °C.

In Figure 1 we show representative high-q (i.e., high scattering angle) scans in the three solid phases. The hexagonal R_{II} phase is characterized by a single peak in this q range. The R_I phase is characterized by two principal peaks in this range. Two temperatures are represented for the R_I phase to emphasize that the R_I phase is not distinguished from the crystal phase by different positions of the peaks, but rather by a very large thermal expansion and temperature dependence of the distortion. The crystal phase (X) has a scattering pattern similar to that of the R_I; however, there is not much change with temperature. In the X phase there is also a weak peak at $q = 2.1$ Å^{-1} assigned to the {210} reflection, which is a signature of the long-range herringbone order of the backbone planes. Schematic representations of the symmetries of the three phases are illustrated in Figure 2. In Figure 2 we also show the reciprocal space peak positions of the principal in-plane reflections (q_1 and q_2 with $q_1 < q_2$) as a function of temperature. The dramatic structural variation in the R_I phase is evident, as are the discontinuities at the two solid−solid transitions.

In Figure 3 we show the area/molecule and the distortion order parameter (ξ) as determined from the peak positions of Figure 2.[8,23] In the orthorhombic R_I and X phases, it is known from the 3D crystal structure, confirmed by the position of the

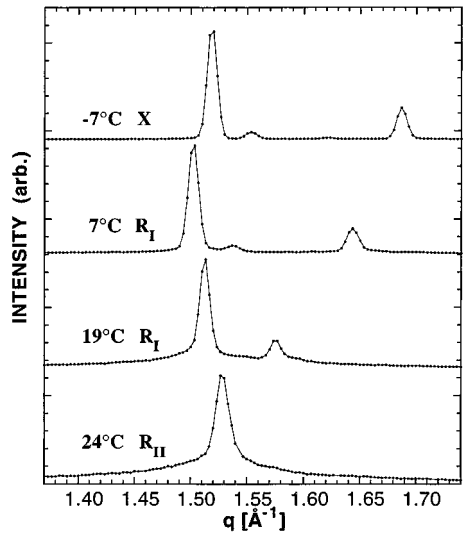

Figure 1. X-ray scans in the high-q range showing typical scattering patterns in the three solid phases. Two extreme temperatures are depicted for the R_I phase.

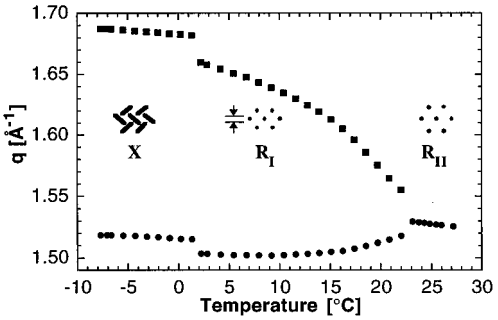

Figure 2. Peak positions of the principal in-plane reflections as a function of temperature. Also shown are schematics illustrating the symmetry of the phases.

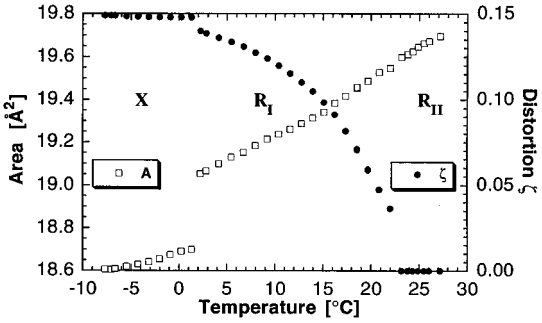

Figure 3. Distortion ξ and the area/molecule as determined from the peak positions of Figure 2.

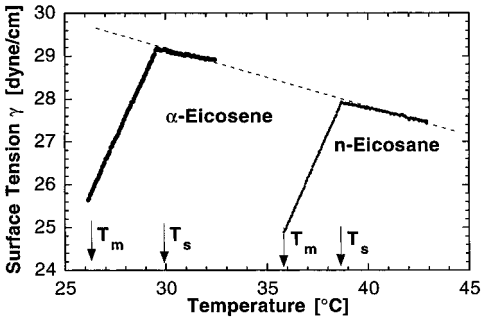

Figure 4. Surface tensions versus temperature for αC20 compared with nC20. The dashed line is a guide to the eye showing that the surface tension curve in the liquid surface phase for αC20 corresponds nearly to that of the extrapolated nC20 curve.

weaker intermediate peak, that the stacking is in an ABA bilayer sequence.[2,4] The projection of the lower peak q_1 onto the plane of the layers is q_1': $q_1' = [q_1^2 - (\pi/d)^2]^{1/2}$. The distortion and area/molecule can be then be calculated: $\xi = 1 - \{[(2q_1'/q_2)^2 - 1]/3\}^{1/2}$ and $A = 8\pi^2/[\sqrt{3}q_2^2(1 - \xi)]$. The larger thermal expansion of the rotator phases[9] is evident here, as well as the jump in area at the transition to the crystal phase. The order parameter ξ increases from 0 at the R_{II} to R_I transition and saturates approaching the crystal phase. The order parameter for the first-order R_I-X transition is not evident from this plot; It is related to the intensity of the {210} reflection, which is zero in the R_I phase and finite in the X phase.[23]

This behavior is very similar to that of the *n*-alkanes; however, the very wide temperature range of the rotator phase is closer to that in *n*-alkane mixtures of a broad chain-length distribution.[25] This wide range (~25 °C) does not occur with small amounts (i.e., 10%) of the neighboring homologues.[25] The wider range in the α-olefin may be due to the reduced interlayer coupling caused by the replacement of the end group and the entropy gained through random inversion of the molecule.

Surface Properties

In Figure 4 we plot the measured surface tension (γ) versus temperature (T) for αC20 and contrast it with that for nC20. The slope of the surface tension gives the difference ΔS in entropy of the surface, S_s, and bulk, S_b, phases: $d\gamma/dT = -(S_s - S_b) = -\Delta S$. For a usual liquid surface, the surface molecules have more freedom than those in the bulk. Hence, $S_s > S_b$ and $d\gamma/dT$ is negative. This is the case for αC20 where $d\gamma/dT = -0.096$ dyn/(cm °C), as it is for nC20 with a very similar $d\gamma/dT = -0.101$ dyn/(cm °C). At a temperature $T_s = 30$ °C, which is 3.4 °C above the bulk freezing point T_m, there is a sharp break in the surface tension curve, characteristic of surface crystallization. The slope changes to one with a very large and positive $d\gamma/dT = 1.06 \pm 0.03$ dyn/(cm °C), a value which is virtually the same as for nC20 within the error bars. This is characteristic of surface crystallization,[17] where the surface layer undergoes ordering into the rotator phase and thus has a much lower entropy. Applying the bulk entropy of melting to a surface layer (using the observed 19.7 Å^2/molecule at melting), we obtain 1.2 dyn/(cm °C), which is very close to the observed slope change of $\Delta(d\gamma/dT) = 1.16$ dyn/(cm °C). This indicates that the slope change is indeed related to the freezing of a monomolecular layer. αC20 deviates from nC20 in the absolute magnitude of the surface tensions. It is apparent, though, that it lies nearly on the value of the surface tension of nC20 extrapolated down to the lower melting temperature of αC20. This behavior is in contrast with short *n*-alkanes, where a lower melting point is always associated with a lower surface tension at melting.[17]

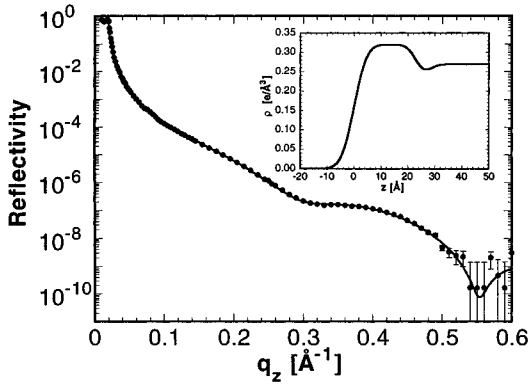

Figure 5. X-ray reflectivity curve from the surface crystalline monolayer at 27 °C. The solid curve is a fit to the form described in the text. The inset shows the electron density profile extracted from the fit parameters.

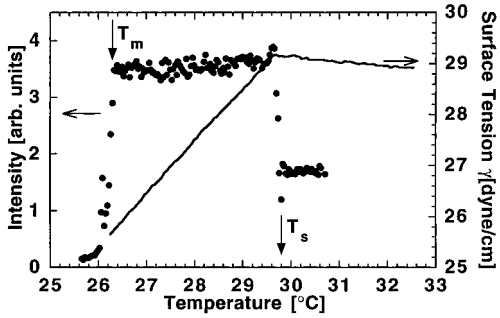

Figure 6. Temperature scan taken on cooling at a rate of 0.2 °C/min, sitting at a fixed incident angle with $q = 0.18$ Å^{-1}. The intensity is constant in the surface crystal phase, indicating no changes to the layer. The constant slope of γ below T_s is another proof for this. Note the agreement of the monolayer formation at T_s and the slope change in γ, showing the latter to result from surface freezing, as discussed in the text.

To characterize the structure of the crystalline surface layer normal to the surface, we measured the X-ray reflectivity as a function of temperature. At temperatures above T_s, the reflectivity is a featureless Fresnel-like curve, typical of liquids.[17] However, at T_s, the reflectivity abruptly becomes modulated as shown in Figure 5. The modulations do not change with temperature within the temperature range of the surface crystal phase (i.e., between T_m and T_s). Since reflectivity is sensitive to electron density, we modeled the electron density at the interface with a two-box model accounting for the body of the monolayer and a depletion region near the interior chain ends.[17] In addition, each interface was allocated a Gaussian roughness parameter. The density profile determined from the fitting with this parametrization is shown in the inset of Figure 5. The thickness of the "body" of the monolayer was thus determined to be 24.3 Å, and the thickness of the depletion region was 1.5 Å. This is consistent with the length of an extended molecule and extremely close to the value for the nC20,[17] which is also extended and normal to the interface.

To determine whether there are strong changes in the structure such as layer thickness or density over the temperature range of the surface crystal phase, we measured the reflected intensity variation with temperature at a judiciously chosen fixed incidence angle. In Figure 6 we show such a T scan at $q = 0.18$ Å^{-1} and a cooling at a rate of 0.2 °C/min. The onset of the surface crystal phase on cooling can be seen by the increase in intensity as the modulation sets in. On bulk crystallization,

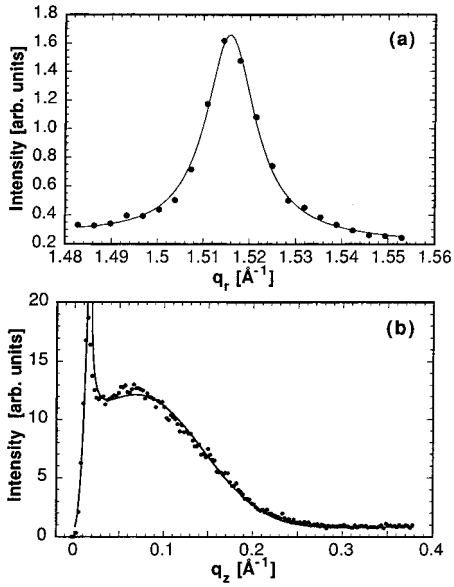

Figure 7. (a) Radial grazing incidence diffraction scan taken at $q_z = 0$ at 27 °C. The solid line is a fit to a Lorentzian shape. (b) A q_z scan through $q_r = 1.516$ Å^{-1}. The solid line is a fit to a general tilted cylinder model.

the surface becomes macroscopically rough, and the intensity decreases dramatically. The intensity is constant throughout the range of stability of the surface crystal phase, showing that the structure and specifically the aspects of the structure which would manifest themselves in a change in the electron density normal to the surface, do not change. These conclusions are also supported by the absence of any slope change in gamma for $T_m < T < T_s$. The agreement between γ and the T scan, as well as that between the temperature at which the slope of γ changes and the jump in the reflectivity at T_s, very strongly supports the interpretation of the slope change as a macroscopic indication for the microscopic formation of the surface monolayer. The ability to detect surface freezing by such a simple standard laboratory method as a surface tension measurement greatly facilitates its study and detection in a variety of systems.

To measure the in-plane structure of the monolayer, we performed grazing incidence diffraction measurements. An in-plane radial scan at $q_z = 0$ in the monolayer phase is shown in Figure 7a. This shows a single peak at $q_r = 1.516$ Å^{-1}, indicating a hexagonal packing also found in the bulk R_{II} rotator phase. A fit to a Lorenztian line shape $I \propto 1(1 + (q - q_p)^2/\Delta q^2)$ gives a peak width of $\Delta q = 0.0065$ Å^{-1}, which is consistent with being resolution limited.[17] A q_z scan through the peak at $q_r = 1.516$ Å^{-1}, known as a "rod scan", is shown in Figure 7b. Rod scans give information on the magnitude and direction of the molecular tilt, as well as the molecular length. The peak at very small q_z is the surface enhancement or "Vineyard" peak which proves that this scattering is originating from the surface and not the bulk. Fitting of the line shape[17] and allowing tilt as a free parameter gives an effective molecular length of 27.6 Å with an upper limit of <6° on the tilt of the molecule from the surface normal. The length is, again, in good agreement with that derived from the reflectivity and the known length of the extended molecule. It is clear from these results that the surface crystal structure is very nearly a monolayer of the R_{II} phase which exists in the bulk below T_m.

Conclusions

The α-olefin α-eicosene behaves similarly to the corresponding *n*-alkane. Shifts of transition temperatures relative to the *n*-alkanes are likely due to the increased entropy and slight energetic cost associated with flipping the molecule whose ends are different. In the range of temperatures studied, no structure reflecting the broken inversion symmetry of the molecule was observed. The results reported here are for the commercially available sample which includes the neighboring homologues and isomers as impurities on the few percent level. On the basis of studies of alkane[25,32] and alcohol mixtures,[27,29,30] we believe that the overall phase behavior regarding rotator phases and surface crystallization is continuous in chain length and not strongly sensitive to this amount of impurity. However, details such as even−odd effects in the structure of the crystal phase, analogous to the triclinic phase which only appears in pure even *n*-alkanes, may be interesting and require a systematic study of a much purer series of α-olefins.

Acknowledgment. We gratefully acknowledge discussions with H. E. King Jr. Part of this work was performed at the National Synchrotron Light Source at Brookhaven National Lab. which is supported by the DOE under Contract DE-AC02-98CH10886. Support by the Israel Science Foundation, Jerusalem, to M.D. and of the Petroleum Research Fund (ACS) to X.Z.W. is gratefully acknowledged.

References and Notes

(1) Ewen, B.; Strobl, G. R.; Richter, D. *Faraday Discuss. Chem. Soc.* **1980**, *69*, 19.
(2) Ungar, G. *J. Phys. Chem.* **1983**, *87*, 689.
(3) Ungar, G.; Masic, N. *J. Phys. Chem.* **1985**, *89*, 1036.
(4) Doucet, J.; Denicolo, I.; Craievich, A. *J. Chem. Phys.* **1981**, *75*, 1523.
(5) Craievich, A.; Denicolo, I.; Doucet, J. *Phys. Rev. B* **1984**, *30*, 4782.
(6) Dorset, D. L.; Moss, B.; Wittmann, J. C.; Lotz, B. *Proc. Natl. Acad. Sci. U.S.A.* **1984**, *81*, 1913.
(7) Maroncelli, M.; Strauss, H. L.; Snyder, R. G. *J. Chem. Phys.* **1985**, *82*, 2811.
(8) Sirota, E. B.; King, H. E., Jr.; Singer, D. M.; Shao, H. H. *J. Chem. Phys.* **1993**, *98*, 5809.
(9) Sirota, E. B.; Singer, D. M.; King, H. E., Jr. *J. Chem. Phys.* **1994**, *100*, 1542.
(10) Sirota, E. B.; Singer, D. M. *J. Chem. Phys.* **1994**, *101*, 10873.
(11) Jimenez, R.; Kruger, J. K.; Prechtl, M.; Grammes, C.; Alnot, P. *J. Phys.: Condensed Matter* **1994**, *6*, 10977.
(12) Yamamoto, T.; Nozaki, K. *Polymer* **1994**, *35*, 3340.
(13) Snyder, R. G.; Srivatsavoy, V. J. P.; Cates, D. A.; Strauss, H. L.; White, J. W.; Dorset, D. L. *J. Phys. Chem.* **1994**, *98*, 674.
(14) Stewart, M. J.; Jarrett, W. L.; Mathias, L. J.; Alamo, R. G.; Mandelkern, L. *Macromolecules* **1996**, *29*, 4963.
(15) Dirand, M.; Achour, Z.; Jouti, B.; Sabour, A.; Gachon, J. C. *Mol. Cryst. Liq. Cryst.* **1996**, *275*, 293.
(16) Wu, X. Z.; Sirota, E. B.; Sinha, S. K.; Ocko, B. M.; Deutsch, M. *Phys. Rev. Lett.* **1993**, *70*, 958.
(17) Ocko, B. M.; Wu, X. Z.; Sirota, E. B.; Sinha, S. K.; Gang, O.; Deutsch, M. *Phys. Rev. E* **1997**, *55*, 3164.
(18) Wu, X. Z.; Ocko, B. M.; Sirota, E. B.; Sinha, S. K.; Deutsch, M.; Cao, B. H.; Kim, M. W. *Science* **1993**, *261*, 1018.
(19) Sirota, E. B.; Wu, X. Z.; Ocko, B. M.; Deutsch, M. *Phys. Rev. Lett.* **1997**, *79*, 531.
(20) Tkachenko, A. V.; Rabin, Y. *Phys. Rev. Lett.* **1997**, *79*, 532.
(21) Earnshaw, J. C.; Hughes, C. J. *Phys. Rev. A* **1992**, *46*, 4494.
(22) Hughes, C. J.; Earnshaw, J. C. *Phys. Rev. E* **1993**, *47*, 3485.
(23) Sirota, E. B. *Langmuir* **1997**, *13*, 3849.
(24) Denicolo, I.; Craievich, A. F.; Doucet, J. *J. Chem. Phys.* **1984**, *80*, 6200.
(25) Sirota, E. B.; King, H. E., Jr.; Shao, H. H.; Singer, D. M. *J. Phys. Chem.* **1995**, *99*, 798.
(26) Clavell-Grunbaum, D.; Strauss, H. L.; Snyder, R. G. *J. Phys. Chem. B* **1997**, *101*, 335.
(27) Sirota, E. B.; Wu, X. Z. *J. Chem. Phys.* **1996**, *105*, 7763.
(28) Deutsch, M.; Wu, X. Z.; Sirota, E. B.; Sinha, S. K.; Ocko, B. M.; Magnussen, O. M. *Europhys. Lett.* **1995**, *30*, 283.
(29) Doerr, A.; Wu, X. Z.; Ocko, B. M.; Sirota, E. B.; Gang, O.; Deutsch, M. *Colloids Surf. A* **1997**, *128*, 63.
(30) Gang, O.; Ocko, B. M.; Wu, X. Z.; Sirota, E. B.; Deutsch, M. *Phys. Rev. Lett.*, **1998**, *80*, 1264.

(31) Hsu, C. S. Hydrocarbons. In *Encyclopedia of Analytical Science*; Wiley: New York, 1995.
(32) Wu, X. Z.; Ocko, B. M.; Tang, H.; Sirota, E. B.; Sinha, S. K.; Deutsch, M. *Phys. Rev. Lett.* **1995**, *75*, 1332.
(33) Kaganer, V. M.; Peterson, I. R.; Kenn, R. M.; Shih, M. C.; Durbin, M.; Dutta, P. *J. Chem. Phys.* **1995**, *102*, 9412.
(34) Small, D. M. *The Physical Chemistry of Lipids*; Plenum: New York, 1986.